Materials Chemistry and Physics 126 (2011) 352–356

Contents lists available at ScienceDirect

Materials Chemistry and Physics

journal homepage: www.elsevier.com/locate/matchemphys

X-ray synthesized PEGylated (polyethylene glycol coated) gold nanoparticles in mice strongly accumulate in tumors

Chang-Hai Wang[a], Chi-Jen Liu[a,*], Chia-Chi Chien[a,b], Hsin-Tai Chen[a], Tzu-En Hua[a], Wei-Hua Leng[a], Hsiang-Hsin Chen[a], Ivan M. Kempson[a], Y. Hwu[a,b,c,**], Michael Hsiao[d], Tsung-Ching Lai[d], J.L. Wang[d], Chung-Shi Yang[e], Hong-Ming Lin[f], Yu-Jen Chen[g], G. Margaritondo[h]

[a] Institute of Physics, Academia Sinica, Nankang, Taipei 115, Taiwan
[b] Department of Engineering and System Science, National Tsing Hua University, Hsinchu 300, Taiwan
[c] Institute of Optoelectronic Science, National Taiwan Ocean University, Keelung 202, Taiwan
[d] Genomic Research Center, Academia Sinica, Nankang, Taipei 115, Taiwan
[e] Center for Nanomedicine, National Health Research Institutes, Miaoli 350, Taiwan
[f] Department of Materials Engineering, Tatung University, Taipei 115, Taiwan
[g] Department of Radiation Oncology and Medical Research, Mackay Memorial Hospital, Taipei 251, Taiwan
[h] Ecole Polytechnique Fédérale de Lausanne (EPFL), CH-1015 Lausanne, Switzerland

ARTICLE INFO

Article history:
Received 16 December 2009
Received in revised form 5 November 2010
Accepted 10 November 2010

Keywords:
Nanoparticle
Biomaterials
Electron microscopy
X-ray microscopy

ABSTRACT

The spatial distribution of X-ray synthesized, PEG coated Au nanoparticles in cancer-bearing mice and their time dependent accumulation were investigated with inductive coupled plasma – optical emission spectroscopy (ICP-OES), transmission electron microscopy (TEM) and histological imaging. The results conclusively demonstrate that the particles strongly accumulate in tumor regions; up to ~25 times more than in normal muscle tissue. This accumulation increases with the time after injection for up to ~12 h in tumor, spleen and liver tissues, whereas for most non-tumor regions it saturates or decreases (blood, lung, brain, heart, and kidney). The impact of this result is discussed with special emphasis on passive targeted drug delivery and could also be used for the delineation and early-stage imaging of small tumors.

1. Introduction

In a series of recent articles [1–6], we announced a new approach for the synthesis of gold nanoparticles coated with PEG ("PEGylated"). The synthesis was activated by irradiation with intense synchrotron X-rays (photon energy 8–15 keV) yielding highly concentrated, stable colloids with no reducing agents. Such nanoparticles could be useful for a number of therapeutical and diagnostic applications.

The PEGylation in this synthesis not only improves the colloidal stability of Au nanoparticles, but also makes the surface functionalization more robust [7]. Of particular note is that the typical thiol-type molecules, often used to provide the link between Au surface and PEG molecules, are not used in this synthesis. Hence the synthesis is much simpler and more controllable. Generation of such particles is potentially important in applications of diagnosing and curing cancer. Specifically, the nanoparticles could improve the selectivity of cancer treatment (chemotherapy and radiotherapy) in targeting cancer areas.

Different approaches have been developed to improve the selectivity in cancer treatments: active targeting, passive targeting and active/passive combinations. Active targeting exploits tumor-specific bio-molecules such as antibodies or functional peptides exhibiting strong affinity for the targeted cells [8–10]. Specific issues in this strategy include: (1) the long time spent in the blood stream; the carriers can direct the payload to unwanted antigens rather than to tumors; and (2) the resistance of the targets to active carriers and the variety of tumor antigens that would require matching a variety of tumor-specific carriers.

Passive approaches, on the other hand, target the specific properties of tumor tissues such as vascular leakage or abnormal vessel architecture. This can facilitate the uptake of specific drug carriers; a property that is called the "enhanced permeation and retention (EPR) effect" [11,12]. Tumors larger than 1–2 mm need new blood vessels to supply nutrients and oxygen which have anomalous density and morphology and ineffective physiological functions (e.g., lymphatic clearance) [12]. For example, for mouse mammary carcinomas the endothelium intercellular openings and the transcellular holes are 1.7 μm and 0.6 μm [13], whereas the size of

* Corresponding author. Fax: +886 2 2651 0704.
** Corresponding author at: Institute of Physics, Academia Sinica, 128 Academia Rd., Sec. 2, Nankang, Taipei 115, Taiwan. Fax: +886 2 2651 0704.
E-mail addresses: cjliuc@phys.sinica.edu.tw (C.-J. Liu), phhwu@sinica.edu.tw (Y. Hwu).

0254-0584/$ – see front matter © 2010 Elsevier B.V. All rights reserved.
doi:10.1016/j.matchemphys.2010.11.014

fenestrations between endothelial cells lining normal blood vessels is only 5–50 nm. These characteristics lead to the EPR effect for suitably small (nano) particles. In turn, such particles could be exploited for targeted drug delivery both for diagnosis and therapy [14–17].

Nanoparticles are being tested in clinical trials as aids in curing cancers and their potential use in diagnosis and therapy is the subject of extensive studies [18–20]. Gold nanoparticles are particularly interesting both for targeted drug delivery [21–24] and radiology contrast or radiotherapy enhancement [25,26]. However, their specific accumulation in tumors has not, so far, been directly demonstrated on a microscopic scale in live animals, although the EPR effect was demonstrated by macroscopic visual observation [9,24] and chemical analysis [25,26].

Our present study sought to provide microscopic evidence that PEG-coated Au nanoparticles strongly accumulate in mice tumors and to compare this to normal muscle tissues. Inductive coupled plasma – optical emission spectroscopy (ICP-OES) was used for determining quantitative Au concentrations associated with specific tissues, while transmission electron microscopy (TEM) and pathological imaging were used to visualize their associations at a cellular level. These microscopy techniques can reveal the evolution of preferential nanoparticle uptake.

2. Experimental

2.1. Gold nanoparticle preparation

PEG modified gold nanoparticles were synthesized by our previously reported synchrotron X-ray irradiation method [1–6]. The exposure was performed at the BL01A beamline of the 1.5 GeV, 300 mA storage ring at NSRRC (National Synchrotron Radiation Research Center), Hsinchu, Taiwan [27]. The PEG–gold nanosols so produced contained spherical gold particles with 6.1 ± 1.9 nm diameter (determined by TEM), were highly concentrated and with excellent colloidal stability within typical *in vitro* and *in vivo* conditions (buffers and whole serum). Other advantages of this synthesis method include the absence of reducing agents and the use of only one solution (with a 0.006 Au/PEG molar ratio). Furthermore, the PEG molecules were not chemically modified to coat the Au surfaces: PEG chains with 6000 molecular weight covered the surfaces. The PEG–gold nanosol was not further functionalized before being injected into the mice.

The colloidal solutions were concentrated by a series of centrifugations with an Eppendorf® 5810R centrifuge and an Amicon® Ultra-15, Millipore centrifugal filter (0.22 μm) device. The final concentration was 26 mg ml^{-1} as determined by the ICP-OES assay (Perkin Elmer Optima-2000 DV).

2.2. Cells and the animal model

EMT-6 syngeneic mammary carcinoma cell lines were cultured in DMEM/F12 medium supplemented with 10% fetal bovine serum, penicillin (100 U ml^{-1}), and streptomycin (0.1 mg ml^{-1}) at 37 °C in a humidified atmosphere containing 5% CO_2. BALB/c ByJNarl mice (5–7 weeks old) were purchased from National Laboratory Animal Center (NLAC) and all procedures involving animals were approved by Academia Sinica Institutional Animal Care and Utilization Committee (AS IACUC). BALB/c ByJNarl tumor models were generated by inoculating 1×10^6 cells in 10 μl phosphate buffered saline (PBS) into the thigh. The mice were used for the study 1 week after inoculation, when the tumor had grown to 50–90 mm^3 (estimated as half the product of the square of the smaller diameter of the tumor multiplied by the larger diameter).

2.3. Biodistribution and blood circulation

Injections, via tail vein, were performed with 200 μl of Au solution. The tumor-bearing mice were sacrificed after the colloidal injection at 0.5, 1.5, 4 or 12 h. A total of 3 mice were used for each time point. After sacrifice, important organs or tissues (blood, lung, tumor, muscle, brain, heart, liver, spleen and kidney) were collected for analysis by ICP-OES (Perkin Elmer Optima 2000 DV, Norwalk, CT), TEM (Hitachi H-7500) and histological analysis.

2.4. TEM sample preparation and observation

To reveal the Au nanoparticle distribution, TEM samples were prepared as follows: the organs were immediately fixed with glutaraldyhyde (Electron Microscopy Sciences, Hatfield, PA) at 4 °C for 24 h. After removing the glutaraldyhyde by 0.1 M PBS, the samples were further fixed and stained with 1% osmium tetraoxide (Electron Microscopy Sciences, Hatfield, PA) in buffer and dehydrated by a series of alcohol treatments, embedded in Spurr's low viscosity resin, and sliced to 90–100 nm in thickness using a Leica Ultracut R ultramicrotome. Initial trimming was with a glass blade and ultrathin sections were prepared with a diamond blade. After being double stained with uranyl acetate and lead citrate, the specimens were observed in a Hitachi H-7500 TEM operating at 100 keV.

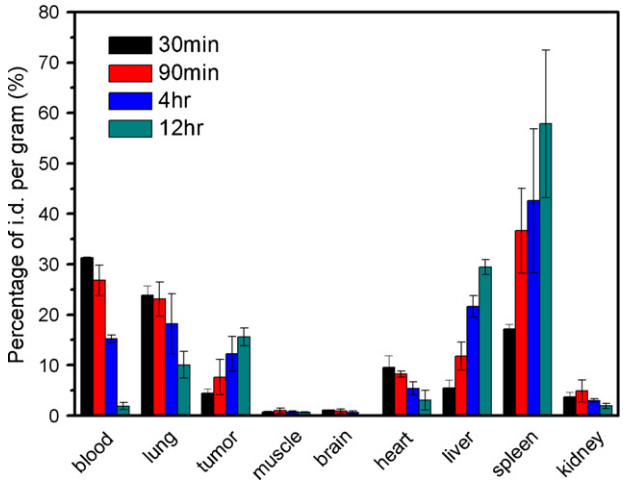

Fig. 1. ICP-OES analysis shows the biodistribution of PEGylated gold nanoparticles in tumor bearing mice for different times after their injection. The results are shown for tumor and non-tumor biopsies.

2.5. Histology analysis

To examine the pathological characteristics of PEG–gold loaded organs/tissues, different organs (tumor, muscle, liver and lung) were immediately fixed in 10% formalin and dehydrated by a series of immersions in 50%, 70%, 90% and, finally, absolute ethanol. The samples were then embedded in paraffin wax and sectioned to 2–5 μm slices with a Leica RM2235 microtome. After histological hematoxylin–eosin (H–E) staining, the slices were observed by an optical microscope (Leica TCS-ST, Germany).

3. Results

3.1. In vivo distribution of PEG–gold nanoparticles

The ICP-OES results indicated that the nanoparticles preferentially accumulated in tumors and revealed specific time-dependent patterns. The gold concentration in all tumors monotonically increased with the time after injection as shown in Fig. 1.

These results reveal that much more gold accumulated in tumor areas than in muscle, brain, kidney or heart tissues. After 4 h, the gold in tumors reached a comparable concentration with that in the blood. The gold concentration in the blood was found to decrease with the time after the exposure, consistent with other pharmacokinetic studies [25,26]. The lung specimen analysis revealed a larger concentration but it decreased with time. For the liver and spleen specimen, substantial gold uptake was observed that increased with time.

The comparison between the tumor and muscle uptake is particularly interesting. Fig. 2 shows the gold concentrations in tumors and muscle and the tumor/muscle uptake ratio after the injection. The Au concentration in the tumor was found to increase significantly with the time for up to 12 h while it saturates or decreases within the muscle, leading to an increase in the tumor/muscle ratio up to ~26.

3.2. Microscopic-scale TEM analysis of the nanoparticle distribution

Visual examination of the tumors indicated a strong accumulation of gold nanoparticles (Fig. 3). TEM was used to determine gold

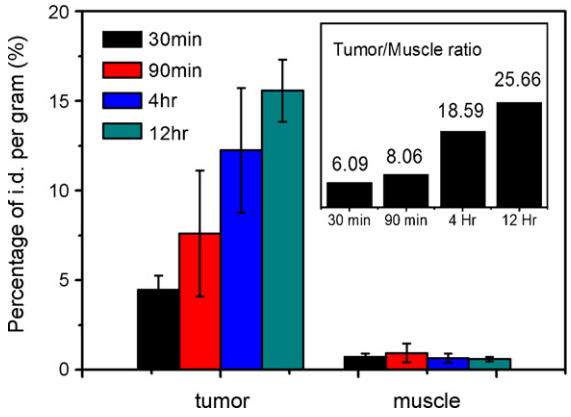

Fig. 2. Enlarged version of the data of Fig. 1 for tumors and non-tumor muscle tissue. The inset shows the tumor/muscle ratio emphasizing its dramatic increase.

associations within the tumor tissue (i.e. to observe if the nanoparticles are incorporated into cells and/or the intercellular matrix). TEM micrographs of various mice organs and tumor are shown in Fig. 4. The individual gold particle size was much larger than that originally administrated. By analogy with other experiments, we believe that this is due to a size increase related to colloidal flocculation and eventual aggregation with other small gold particles [1]. Large quantities of nanoparticles are internalized in the vesicle within the cytoplasm for almost all of the observed tissues. However, nanoparticles were not found inside the cell nuclei. For example, the distribution of gold in liver is shown in Fig. 4(b). It was found that gold particles aggregated in the endosome were confined within the cytoplasm of the liver cells.

3.3. Histology imaging

Fig. 5 shows microscopy images of tumor, muscle, liver and lung after H–E staining. Large amount of Au nanoparticles (the dark regions) was found in the cross-sectional view of a small blood vessel within the tumor containing region (Fig. 5(a)). Some nanoparticles are also observed in the neighboring inter-cellular matrix. For the muscle tissue (Fig. 5(b)), a lesser amount of Au nanoparticles was found in the skeletal muscle and eosinophilic cytoplasm. Fig. 5(c) shows the nanoparticle distribution within the network-like lobules of the liver. The images indicate the formation of nanoparticle aggregates. The Kupffer cells within the lobule captured the nanoparticle aggregates. Flake-like, large gold aggregates also appeared within the non-tumor micro-vasculature of lung, as shown in Fig. 5(d). The aggregates were found adhered to vessel walls.

In essence, the histology imaging results confirmed that large amounts of PEGylated gold nanoparticles accumulated in tumors, lungs and the reticuloendothelial system (RES, i.e. the liver and spleen), consistent with the ICP-OES and TEM data. The histology images did not detect any pathological changes related either to inflammation or to active immunocyte congregation in these organs.

4. Discussion

Previous experiments on gold nanoparticle accumulation in live animal organs revealed interesting accumulation effects in tumors but did not bring to light the positive effects of PEGylation [25,26]. Hainfeld et al. evaluated the biodistribution of highly concentrated Au nanoparticles in tumor-bearing mice [25,26]. They found that the maximum nanoparticle concentration in tumors was at ≈7 min after injection, followed by a slower concentration decrease than for other organs. After 5 min, the tumor-to-muscle Au ratio was 3.5 whereas the kidney-to-tumor ratio was 27. Au particles completely left the muscle tissue and the blood 24 h after the injection, whereas tumors still retained a substantial gold accumulation.

The PEGylated nanoparticles used here demonstrated significantly different accumulation dynamics. The dissimilarities could be caused by differences in the particle dimension, surface chemistry and administrated dose that could influence both the RES uptake and the EPR effect.

The actual occurrence of the EPR effect depends on several prerequisites: (a) high stability and high concentration; (b) no fast evacuation by renal clearance or RES capture; (c) in general, a long circulation time. Concerning the nanoparticle size, we adopted the 6 nm value that falls in the optimal size range to achieve high concentrations at tumor sites based on the EPR effect [25,26]. Au nanoparticles with much smaller size (≈1.9 nm) were selected by Hainfeld et al. to avoid a large liver uptake [25,26]. However, we found that our 6 nm nanoparticles have comparable concentrations in tumors and liver 90 min after injection and, contrary to smaller particles, the Au concentration in tumors tended to increase afterwards. These facts support our size choice of slightly larger nanoparticles.

PEGylation of nanoparticle surfaces is quite effective in enhancing the effectiveness of tumor targeting [28]. The immobilization of the PEG chains on the surfaces forms hydrophilic brushes that prevent opsonins from recognizing the particles and inhibiting the phagocytosis by the RES cells. Efforts in that sense were concentrated on liposome and polymeric nanoparticles. Paciotti et al.

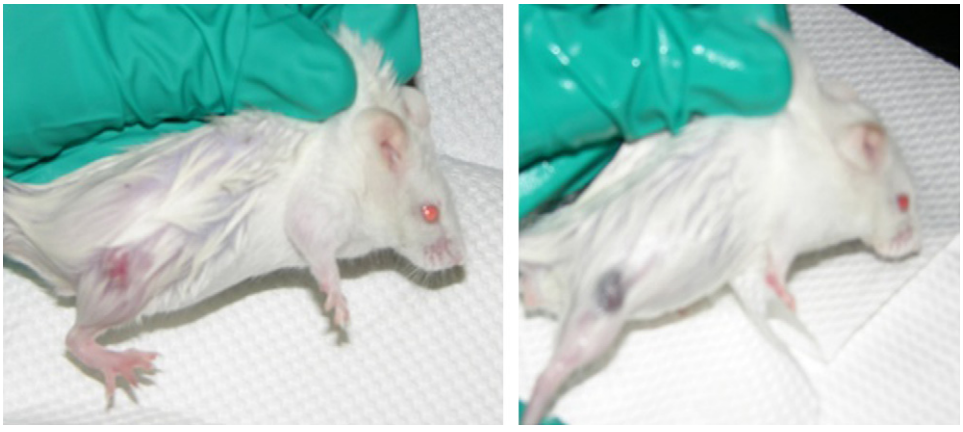

Fig. 3. Photo images visually showing the strong accumulation of PEGylated gold nanoparticles in tumor sites after the tail vein injection; the left picture was taken before injection and the right image 24 h after injection.

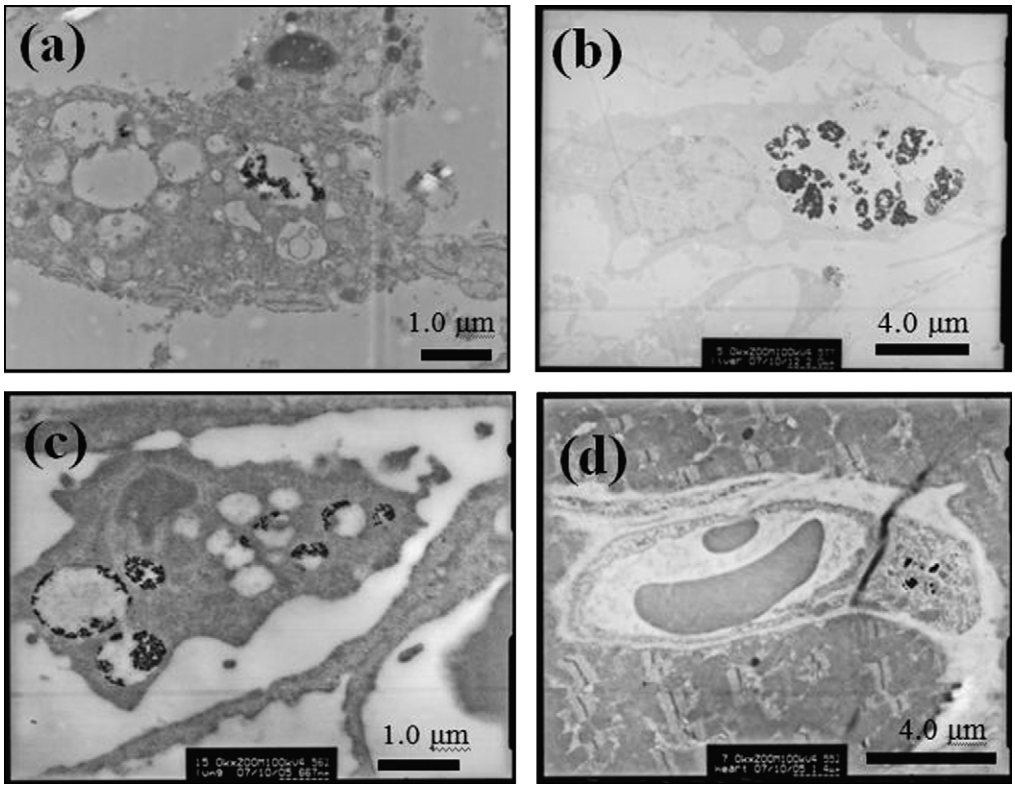

Fig. 4. TEM micrographs of different regions with accumulated PEGylated Au particles 24 h after injection: (a) tumor; (b) liver; (c) lung; (d) heart.

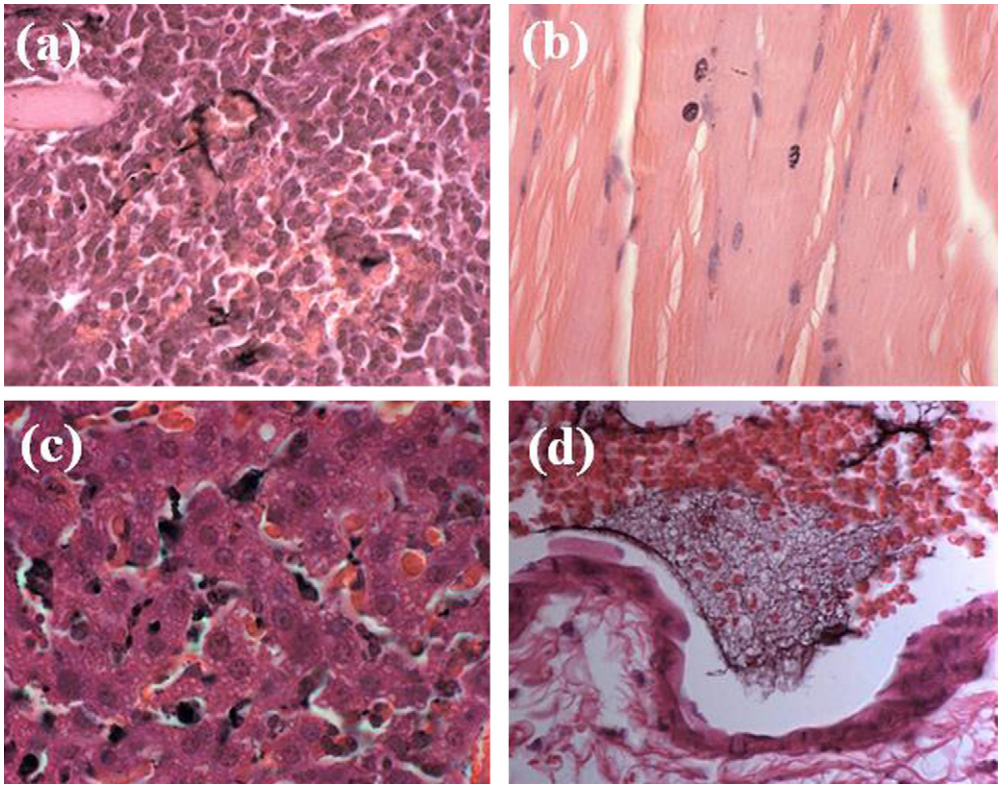

Fig. 5. Histology images (40×) of PEGylated Au particles in different organs 24 h after injection: (a) tumor; (b) muscle; (c) liver; (d) lung.

proposed PEGylated gold nanoparticles for targeted drug delivery [8,24]. They specifically used PEGylation to improve the anti-tumor effectiveness of TNF-α and Paclitaxel. Thus, the tumor targeting was a combined effect of passive targeting by PEGylated gold and active targeting of TNF-α, making it difficult to isolate the specific effects of PEGylation.

Here we adopted a very simple approach based only on PEGylation and found that the PEGylated particles passively accumulate within tumors. Besides targeted drug delivery, these findings could have an important impact on other aspects of diagnosis and therapy. In fact, the strong accumulation of gold within tumors could facilitate their radiological imaging as well as nanoparticle-enhanced irradiation therapy.

5. Conclusion

Our combined quantitative ICP-OES and microscopy tests demonstrated that 6 nm PEGylated gold particles are strongly concentrated in tumors in mice. After 12 h this concentration is ∼25 times larger than in normal muscle tissues, but approximately one half to one third of that for RES organs. This direct evidence could warrant the possible use of PEGylated gold nanosols, in particular those prepared by X-ray irradiation, for targeted drug delivery, radiotherapy and radiological diagnosis.

Acknowledgements

This work was supported by the National Science and Technology Program for Nanoscience and Nanotechnology, the Thematic Research Project of Academia Sinica, the Biomedical Nano-Imaging Core Facility at National Synchrotron Radiation Research Center (Taiwan), the Center for Biomedical Imaging (CIBM) in Lausanne, partially funded by the Leenaards and Jeantet foundations and by the Swiss Fonds National de la Recherche Scientifique and by the EPFL.

References

[1] C.H. Wang, T.E. Hua, C.C. Chien, Y.L. Yu, T.Y. Yang, C.J. Liu, W.H. Leng, Y.K. Hwu, Y.C. Yang, C.C. Kim, J.H. Je, C.H. Chen, H.M. Lin, G. Margaritondo, Mater. Chem. Phys. 106 (2007) 323.
[2] Y.C. Yang, C.H. Wang, Y. Hwu, J.H. Je, Mater. Chem. Phys. 100 (2006) 72.
[3] C.J. Liu, T.Y. Yang, C.H. Wang, C.C. Chien, S.T. Chen, C.L. Wang, W.H. Leng, Y. Hwu, H.M. Lin, Y.C. Lee, C.L. Cheng, J.H. Je, G. Margaritondo, Mater. Chem. Phys. 117 (2009) 74.
[4] C.J. Liu, C.H. Wang, C.C. Chien, T.Y. Yang, S.T. Chen, W.H. Leng, C.F. Lee, K.H. Lee, Y. Hwu, Y.C. Lee, C.L. Cheng, C.S. Yang, Y.J. Chen, J.H. Je, G. Margaritondo, Nanotechnology 19 (2008) 295014.
[5] C.H. Wang, C.C. Chien, Y.L. Yu, C.J. Liu, C.F. Lee, C.H. Chen, Y. Hwu, C.S. Yang, J.H. Je, G. Margaritondo, J. Synchrot. Radiat. 14 (2007) 477.
[6] C.H. Wang, C.J. Liu, C.L. Wang, T.E. Hua, J.M. Obliosca, K.H. Lee, Y. Hwu, C.S. Yang, R.S. Liu, H.M. Lin, J.H. Je, G. Margaritondo, J. Phys. D 41 (2008) 195301.
[7] T.M. Allen, Nat. Rev. Cancer 2 (2002) 750.
[8] G. Zhang, Z. Yang, W. Lu, R. Zhang, Q. Huang, M. Tian, L. Li, D. Liang, C. Li, Biomaterials 30 (2009) 1928.
[9] G.F. Paciotti, L. Myer, D. Weinreich, D. Goia, N. Pavel, R.E. Mclaughlin, L. Tamarkin, Drug Deliv. 11 (2004) 169.
[10] Z. Liu, W. Cai, L. He, N. Nakayama, K. Chen, X. Sun, X. Chen, H. Dai, Nat. Nanotechnol. 2 (2007) 47.
[11] K. Iwai, H. Maeda, T. Konno, Cancer Res. 44 (1984) 2115.
[12] Y. Matsumura, H. Maeda, Cancer Res. 46 (1986) 6387.
[13] L.W. Seymour, Y. Miyamoto, H. Maeda, M. Brereton, J. Strohalm, K. Ulbrich, R. Duncan, Eur. J. Cancer 31 (1995) 766.
[14] T. Konno, H. Maeda, K. Iwai, S. Tashiro, S. Maki, T. Morinaga, M. Mochinaga, T. Hiraoka, I. Yokoyama, Eur. J. Cancer Clin. Oncol. 19 (1983) 1053.
[15] T. Konno, H. Maeda, K. Iwai, S. Maki, S. Tashiro, M. Uchida, Y. Miyauchi, Cancer 54 (1984) 2367.
[16] H. Maeda, Adv. Drug Deliv. Rev. 6 (1991) 181.
[17] H. Maeda, K. Greish, J. Fang, Adv. Polym. Sci. 193 (2006) 103.
[18] V.P. Zharov, E.N. Galitovskaya, C. Johnson, T. Kelly, Lasers Surg. Med. 37 (2005) 219.
[19] M. Ferrari, Nat. Rev. Cancer 5 (2005) 161.
[20] I.H. El-Sayed, X.H. Huang, M.A. El-Sayed, Cancer Lett. 239 (2006) 129.
[21] J.L. West, N.J. Halas, Curr. Opin. Biotechnol. 11 (2000) 215.
[22] S.R. Sershen, S.L. Westcott, N.J. Halas, J.L. West, J. Biomed. Mater. Res. 51 (2000) 293.
[23] L. Ren, G.M. Chow, Mater. Sci. Eng. C 23 (2003) 113.
[24] G.F. Paciotti, D.G.I. Kingston, L. Tamarkin, Drug Dev. Res. 67 (2006) 47.
[25] J.F. Hainfeld, D.N. Slatkin, H.M. Smilowitz, Phys. Med. Biol. 49 (2004) N309.
[26] J.F. Hainfeld, D.N. Slatkin, T.M. Focella, H.M. Smilowitz, Br. J. Radiol. 79 (2006) 248.
[27] G. Margaritondo, Y. Hwu, J.H. Je, Riv. Nuovo Cimento 27 (2004) 7.
[28] L.E.V. Vlerken, K.V. Tushar, M.M. Amiji, Pharm. Res. 24 (2007) 1405.